Stray-field effects in submicron $YBa_2Cu_3O_{7-x}$ bicrystal grain boundary junctions

G. Testa,[1] F. Laviano,[2] D. -J. Kang,[3] E. J. Tarte,[4] S. H. Mennema,[5] and M. G. Blamire[5]
[1]*Istituto di Cibernetica "E.Caianiello" del CNR, Via Campi Flegrei 34, 80078 Pozzuoli (Naples), Italy*
[2]*Department of Physics, Politecnico di Torino, C.so Duca degli Abruzzi 24, 10129 Torino, Italy*
[3]*Nanoscience Centre, IRC in Nanotechnology, Cambridge CB3 0FF, United Kingdom*
and Sungkyunkwan Advanced Institute of Nanotechnology and Department of Physics, Sungkyunkwan University, Suwon 440-746, Korea
[4]*Department of Electrical Engineering, University of Birmingham, Birmingham B15 2TT, United Kingdom*
[5]*Department of Materials Science, University of Cambridge, Pembroke Street, Cambridge CB2 3QZ, United Kingdom*
(Received 18 October 2005; published 24 January 2006)

We have investigated the magnetic field dependence of the critical current in submicron $YBa_2Cu_3O_{7-x}$ [001] tilt bicrystal grain boundary junctions. The good homogeneity of submicron grain boundary barrier interfaces, together with the large magnetic field needed to modulate the Josephson current, allow to observe several features not observed in micron size junctions, like a nonconstant modulation period, strongly dependent on the maximum applied magnetic field. Experimental results are well accounted for by a theoretical model taking into account the magnetization of the nearby electrode, and the strong interaction of its stray field with the junction interface. The analysis of the nature of this interaction and the influence of the device geometry are also relevant for potential applications of high critical temperature LSI devices.

DOI: 10.1103/PhysRevB.73.014522 PACS number(s): 74.50.+r, 74.20.Rp, 74.72.−h

I. INTRODUCTION

The magnetic field dependence of the critical current $I_{Cj}(H_a)$, where H_a is the external applied magnetic field, is one of the most powerful diagnostic tool for the properties of superconducting Josephson junctions.[1] It can give information on the barrier uniformity,[1] on the effect of trapped Abrikosov vortices,[2–8] or even on the order parameter symmetry of the superconducting electrodes.[9–11]

While in good conventional superconducting Josephson junctions the $I_{Cj}(H_a)$ dependence follows a clear "Fraunhofer" pattern:

$$I_{Cj}(H_a) = I_{Cj}(0)\left|\frac{\sin(\pi\Phi/\Phi_0)}{\pi\Phi/\Phi_0}\right| \quad (1)$$

its behavior is much more complicated in high critical temperature superconducting (HTS) grain boundary junctions (GBJs).[12] Even limiting our investigation to misorientation angles for which the contribution of the unconventional *d*-wave order parameter symmetry is negligible, the $I_{Cj}(H_a)$ dependence is generally very irregular because of the nonuniform nature of the barrier interface.[12–15] Moreover, the planar structure typical of most HTS GBJs leads to a w^{-2} dependence of the modulation period,[16] where w is the junction width, in contrast to the w^{-1} dependence measured in low critical temperature conventional junctions.

Most of the studies on the magnetic properties of GBJs take only into account the current distribution inside the barrier interface[1] and also when the effect of the adjacent electrodes is considered, it is generally limited to the "small field" (Meissner region) and "large field" (uniform vortex density) cases.

In this paper, we investigate, both experimentally and theoretically, the interaction of submicron bicrystal grain boundary junctions with the electrodes in their "intermediate case," i.e., when vortices start penetrating the thin films and their density and position increase as a function of the externally applied magnetic field. For this analysis the use of submicron junctions[17] is very helpful for two main reasons: (i) large magnetic fields needed to modulate their critical current make a large number of vortices enter the electrodes and interact with the junction barrier, and (ii) the reduced junction size results in relatively more uniform barrier interfaces, as demonstrated in previous experiments on transport and interface properties.[18–20] Submicron GBJs become then a tool to study the vortex dynamics and the magnetization of superconducting thin films.

The analysis of the interaction of vortices with the grain boundary interface and the influence of the device geometry are also relevant for applications of HTS devices, from digital integrated circuits to HTS SQUID magnetometers, whose $1/f$ low frequency noise is strongly influenced by trapping and hopping of vortices close to the SQUID body.

II. THEORETICAL DESCRIPTION

The penetration of magnetic fields in thin slabs and discs has been widely studied and discussed with both numerical and analytical calculations (within the Bean[21,22] assumption, critical current density J_C=constant), also in the presence of current transport.[23,24]

In our experiments, we are considering thin films in perpendicular applied magnetic fields H_a.[23,24] In such configurations, demagnetization effects are very important. Assuming a long flat strip, with thickness $d<w$ (linewidth), and rectangular cross section, $|z|<d/2$, $|y|<w/2$, the current density J in the electrodes is expected to be strongly related to the curvature of flux lines. Indeed, also for weak applied magnetic fields, when there is no penetration of the perpendicular component B_z, the net magnetic field wraps around the film and the tangential B_y component is characterized by opposite values at the two outer film surfaces (top and

bottom).[25] In this "transverse geometry," the screening currents do not flow only along a small depth, of the order of λ from the edge, where λ is the London penetration depth (for thin films we should consider an effective penetration depth $\lambda_{\text{eff}}=2\lambda^2/d$), but down to the middle of the sample. Moreover, the exact current density distribution over the sample thickness is irrelevant. Indeed, being in our films $d<2\lambda$, J_C is almost constant over the whole thickness. The current component perpendicular to the film plane is negligible compared to the other two and the current distribution can be considered as two dimensional (2D), $\vec{J}=\hat{x}J_x+\hat{y}J_y$. In this case, the total current

$$I(x,y)=\int_{-d/2}^{d/2} J(x,y,z)dz$$

can be calculated as $I(x,y)=dJ(x,y)$. Such current, flowing along the strip, generates a magnetic self-field which adds to the external applied field. At $z=\pm d/2$, its perpendicular component is characterized by a nonlocal relationship,[26]

$$H_z(y)=\int_{-w/2}^{w/2}\frac{I(u)du}{y-u}$$

while the parallel component is determined only by the closest current path, $H_y(y)=\frac{1}{2}I(y)\text{sgn}(z)$.

Because of demagnetization effects, a logarithmic overshooting $H_{\text{edge}}>H_a$ then appears close to the sample edge, i.e., the field at the film edge is much larger than the applied field. When $H_{\text{edge}}>H_{c1}$ (the lower critical field), quantized vortices (fluxons) nucleate at the film edge, where the Lorentz force $F=qJ\times B$ is maximum, and penetrate the film. Such a flux entry is regulated by three main factors: the driving Lorentz force, the pinning force associated to structural defects, and the surface barrier to flux penetration. The role of surface barriers can however be neglected in the case of strong pinning.

Once penetrated, a vortex is pushed inside the film until it meets a structural defect on its trajectory, where the electromagnetic force is balanced by the pinning force (larger penetration for weaker pinning). By increasing the magnetic field more vortices enter the film. Considering the small thickness $d\sim\lambda$, such vortices have Pearl-like structure.[27] They interact mainly via their stray field, which generates a current density in the film decreasing as $1/r$ at large distances r. The force between two such "Pearl vortices," containing one flux quantum Φ_0, is then long range, $J\Phi_0 d\propto 1/r$ and the electromagnetic interaction, expected in our thin films, is then much larger than in the superconducting bulk, as calculated by Carneiro and Brandt.[28]

When the external magnetic field H_a is reduced to zero and there is no Lorentz force from the shielding currents, the vortex remains trapped at the pinning center (if the pinning strength is large enough to avoid that the mutual repulsion among vortices leads to some flux expulsion). By applying an opposite magnetic field $-H_a$, the vortex is swept out from the film and a new vortex, of opposite sign, will be placed at the same irregularity. It is worth noting that the flux escape is blocked by a surface barrier that does not disappear until Ha is reduced to zero.[21,22] A surface hysteresis, related to the delayed flux expulsion, is then expected at decreasing fields.

In this paper, we will follow the theoretical macroscopic approach described in Ref. 24, referring to thin strips in perpendicular magnetic fields. In this model, the calculated initial flux penetration is quadratic in H_a, i.e., there is a delay in the entrance of vortices in the strip, like it would be in the presence of a first critical field $H_p\simeq 0.296H_c$. It is worth noting that the results of such macroscopic theory are consistent with the microscopic details considered in Ref. 28.

The field profiles are calculated, for both increasing applied magnetic fields H_{inc} (from zero to a maximum value H_{max}) and for decreasing fields, H_{dec}, from H_{max} to $-H_{\text{max}}$, by using Eqs. (2) and (3), respectively. In the calculations, the critical sheet current $J_C d$ is assumed constant, i.e., independent of the local flux density, and $H_{c1}=0$,

$$H_{\text{inc}}=\begin{cases}0 & \text{for } |y|<b,\\ \dfrac{J_C d}{\pi}\arctan h\dfrac{\sqrt{(y^2-b^2)}}{c|y|} & \text{for } b<|y|<w,\\ \dfrac{J_C d}{\pi}\arctan h\dfrac{c|y|}{\sqrt{(y^2-b^2)}} & \text{for } |y|>w,\end{cases} \tag{2}$$

$$H_{\text{dec}}(y,H_a,J_C)=H(y,H_{\text{max}},J_C)-H(y,H_{\text{max}}-H_a,2J_C), \tag{3}$$

where $b=w/\cosh(H_a/H_c)$ is the Meissner flux-free region and $c=\tanh(H_a/H_c)$.

In Fig. 1, we show the simulated profiles of a superconducting strip, 500 μm large and 120 nm thick, when [Fig. 1(a)] a magnetic field is increased from 0 to several H_{max} values and [Fig. 1(b)] at several decreasing H_a, from 100 Oe to −100 Oe. We can see a continuous penetration of vortices for increasing applied magnetic fields while, in the decreasing magnetic field branch, the strayfield of trapped vortices, which is strongly dependent on H_{max}, creates a negative field at the strip edge even for positive H_a values. In both cases, we see the logarithmic discontinuity at the strip edge and a strong stray field, far outside the sample. From the above considerations we can then conclude that, if a Josephson junction[1] is patterned close to the electrode, we may expect a relevant contribution of such a stray field (including vortex and Meissner currents) on the junction properties. Physically, vortices tend to arrange in the electrode by a Bean-Livingstone[21] type interaction and their number and position, affected by structural geometrical conditions and pinning, will modify the critical current distribution into the junction.

III. EXPERIMENTAL PROCEDURES

Submicron grain boundary junctions have been fabricated according to the following procedure. A stack of 120–140 nm thick $YBa_2Cu_3O_{7-x}$ film and a protective 50 nm thick amorphous $SrTiO_3$ layer have first been deposited, by laser ablation, on symmetric 24° [001] tilt $SrTiO_3$ bicrystal substrates. These two films have then been covered by a gold layer, 50 nm thick, in order to have a conductive

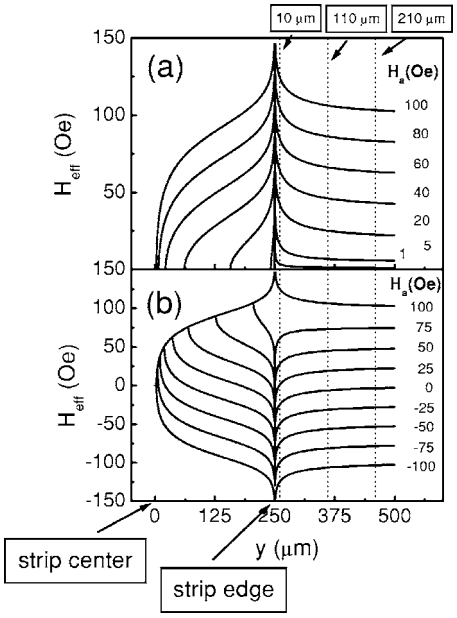

FIG. 1. Simulated profiles of a superconducting strip (half of the full width is shown) in a perpendicular magnetic field, according to Ref. 24. The width of the strip is 500 μm and its thickness 120 nm. (a) The increasing applied magnetic fields cause penetration of vortices. (b) In the decreasing magnetic field branch, the trapped vortices depends on the maximum applied field. In both cases, a strong stray field, far outside the sample is present. The magnetic field at the strip edge is characterized by a logarithmic discontinuity due to the "transverse geometry." The dotted vertical lines give the effective magnetic field values at distances of 10 μm, 110 μm, 210 μm, respectively, from the strip edge.

film for the FIB process. The device geometry has been defined by standard photolithography and Ar ion beam milling etch. The mask used allowed to obtain 44 junctions with widths ranging from 2 μm to 20 μm. A number of junctions have then been narrowed, in the range 0.3–1 μm, by using a FIB microscope with a Ga source. Figure 2(a) shows the final device pattern and Fig. 2(b) a FIB picture of a typical submicron grain boundary junction, just after the focused ion beam etch (the solid line indicates the bicrystal line, not visible under the FIB). A more detailed description of the fabrication procedure is reported elsewhere.[17]

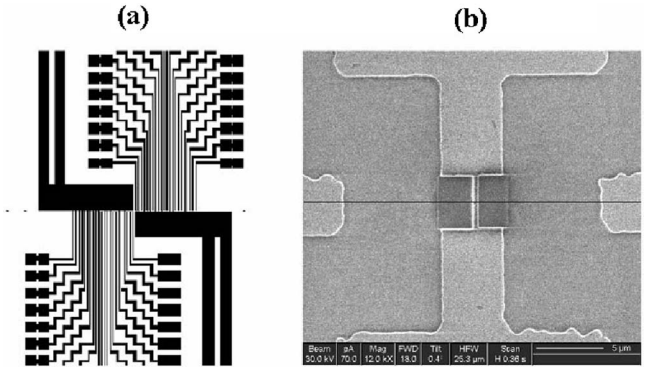

FIG. 2. (a) Final device pattern. 44 junctions ranging from 0.3 to 20 μm have been defined. (b) FIB picture of a typical submicron grain boundary junction, just after the focused ion beam etch (the solid line indicates the bicrystal line, not visible under the FIB).

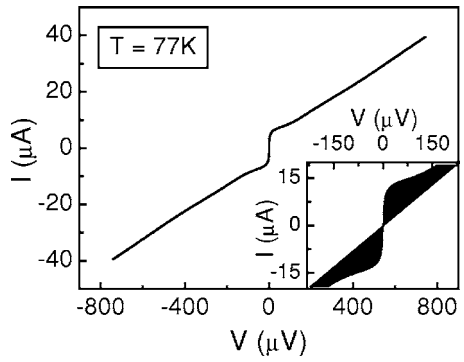

FIG. 3. Current-voltage characteristic of a 400 nm wide GBJ at $T=77$ K. In the inset, current voltage characteristics of a 470 nm wide junctions with applied magnetic fields in the range −50 Oe–50 Oe.

All the experiments have been made, with very low noise electronics, in a helium cryostat shielded by 1 thick aluminum and 3 μ-metal shields with a residual field lower than 1 mOe. Samples have been measured both in liquid helium ($T=4.2$ K) and in liquid nitrogen ($T=77$ K) by using a vacuum probe covered by both a superconducting lead cylinder and a cryoperm shield. The external magnetic field (up to 100 Oe at $T=77$ K and 350 Oe at $T=4.2$ K) has been applied by a copper solenoid with the main axis normal to the film plane.

IV. EXPERIMENTAL RESULTS AND DISCUSSION

Current-voltage (I-V) characteristics of all our submicron bicrystal grain boundary junctions are well accounted for by the resistively shunted junction (RSJ) model, including a thermal rounding noise.[1] Figure 3 shows a typical I-V characteristic at $T=77$ K. The critical current densities J_{Cj} are of the order of 10^4 A/cm^2 at $T=77$ K and about $2-5\times10^5$ A/cm^2 at $T=4.2$ K.[17] One important feature is the complete suppression of the critical current by applying external magnetic fields (inset of Fig. 3). This property is a clear signature of the improvement of the barrier homogeneity obtained by reducing the junction widths, as also evidenced by experiments on Andreev bound states in 45° [001] symmetric GBJs.[1,18,19]

However, the $I_{Cj}(H_a)$ measured in our submicron junctions differs from the typical Fraunhofer pattern, Eq. (1), in a number of respects. In Fig. 4, a typical $I_{Cj}(H_a)$ behavior at $T=77$ K is shown for a 700 nm wide junction. By increasing the magnetic field, from 0 to a maximum value $H_{max}=100$ Oe, the modulation pattern shows a nonconstant period, in contrast to what is expected in a Fraunhofer pattern. In particular, in Fig. 4, the second period is larger than the first one. This effect is more evident when the magnetic field decreases from H_{max} to $-H_{max}$.

In Fig. 5, the $I_{Cj}(H_a)$ dependencies for a 1 μm wide GBJ are shown for several H_{max} values. In all the curves the magnetic field was changed from 0 to H_{max} (before starting the

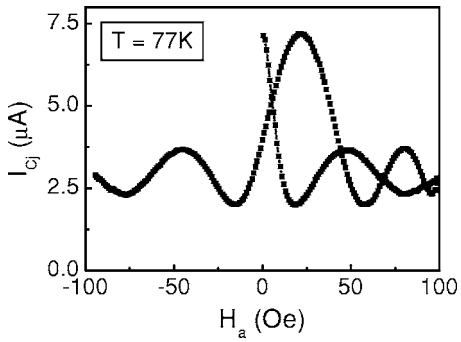

FIG. 4. Dependence of the critical current on the magnetic field for a 700 nm wide GBJ at $T=77$ K. The magnetic field has been varied from 0 to $H_{max}=100$ Oe and then from H_{max} to $-H_{max}$.

measurements), then from H_{max} to $-H_{max}$. The most interesting effect is that curves do not overlap and are not simply shifted along the magnetic field axis. Limiting our attention only to positive currents (for negative currents the discussion is completely equivalent), and moving from H_{max} to $-H_{max}$, the first period slightly increases with H_{max} while the central period strongly depends on the maximum applied field (it doubles by changing H_{max} from 10 Oe to 50 Oe). Finally, all the curves reach their minimum at the same negative field value, and overlap when the magnetic field is increased in the negative direction. This effect is perfectly reproducible;

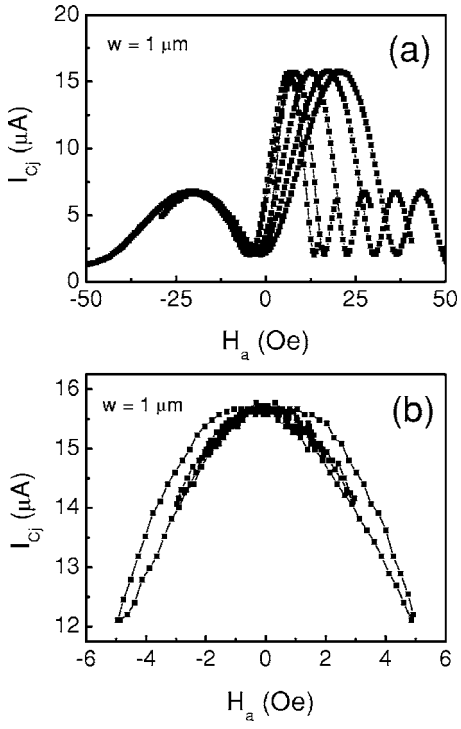

FIG. 5. (a) Dependence of the critical current on the magnetic field for a 1 μm wide GBJ at $T=77$ K. The different curves refer to different H_{max} values, ranging from 0.1 Oe to 50 Oe. In all these curves the magnetic field has been changed from 0 to H_{max} (before starting measurements), then from H_{max} to $-H_{max}$ and finally from $-H_{max}$ to H_{max} with the current inverted. (b) $I_{Cj}(H_a)$ at small fields. A field threshold of about 3 Oe for the appearance of the hysteresis is clearly visible.

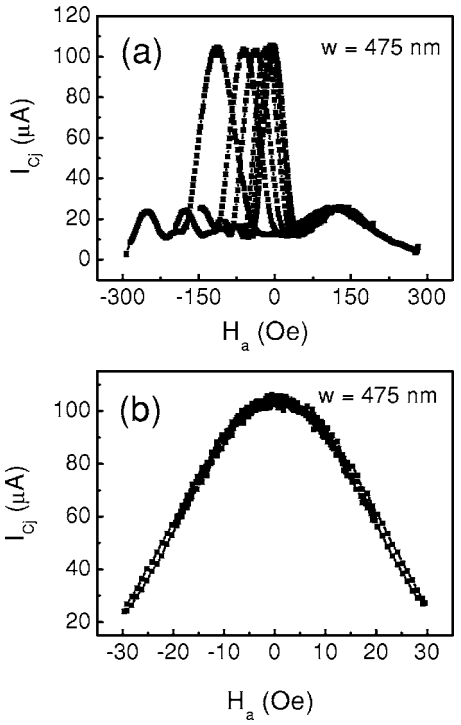

FIG. 6. (a) Dependence of the critical current on the magnetic field for a 475 nm wide GBJ at $T=4.2$ K. The different curves refer to different H_{max} values, ranging between 0.1 Oe and 300 Oe. In all these curves the magnetic field has been changed from 0 to H_{max} (not reported in the figure), then from H_{max} to $-H_{max}$ and finally from $-H_{max}$ to 0. (b) $I_{Cj}(H_a)$ at small fields. At this temperature, the field threshold is of the order of 30 Oe.

we have measured the same sample, some weeks after with a different probe, obtaining exactly the same curves. It is worth noting that, in Figs. 4 and 5, the critical current does not go to zero only because a voltage threshold criterion has been used to estimate I_{Cj}.

The not constant modulation period is always accompanied by a shift of H_{peak}, defined as the magnetic field value corresponding to the maximum critical current. H_{peak} is positive when H_a is decreased from H_{max} and negative when the applied magnetic field goes from $-H_{max}$ to 0.

All these effects have also been observed at $T=4.2$ K, as shown in Fig. 6 for a 475 nm wide GBJ.

In Fig. 7, we show both the shift in H_{peak} and the central modulation period as a function of H_{max} for two junctions, 770 nm and 1 μm wide, respectively. It is worth noting that both the shift and the width of the central peak show a similar dependence on the maximum applied magnetic field, indicating the same physical mechanism. However, while the first modulation period scales with the junction width, the shift is constant for both 770 nm and 1 μm junctions. Therefore, H_{peak} does not depend on the junction width in contrast to what is reported in the literature.[7]

The shift in H_{peak} is significant only for magnetic fields larger than a threshold value H_{th}, of the order of a few Oersted at $T=77$ K [Fig. 5(b)] and some tenths of Oe at $T=4.2$ K [Fig. 6(b)], independently of the junction width.

A positive H_{peak} for decreasing magnetic fields is consistent with the presence of a number of vortices trapped in the

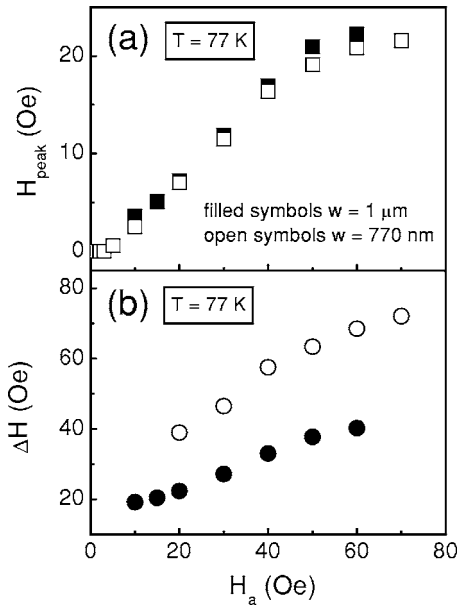

FIG. 7. Dependence of the hysteresis and the central period on the maximum applied magnetic field H_{max}, for a 770 nm wide (open symbols) and a 1 μm wide GBJ (filled symbols), respectively. Data refer to $T=77$ K.

superconducting electrodes, which give a contribution to the total magnetic field sensed by the junction opposite with respect to the external one. Indeed, if vortices were trapped in the junction area, they would sum their stray field to the external one, giving a peak at negative values.[3,6–8,29]

In Ref. 29, the hysteretic $I_{Cj}(H_a)$ behavior was accounted for by a model, based on the Ginsburg-Landau equation, which considers the transverse geometry of the thin film junction and the contribution of both Meissner currents and Abrikosov vortices (with and without pinning) close to the grain boundary. This model relates the hysteretic $I_{Cj}(H_a)$ behavior to the hysteretic nature of the contribution of Abrikosov vortex to supercurrents. However, it predicts a dramatic increase of the period above H_{C1}, because of the entrance of vortices with a contribution opposite to the Meissner shielding current. Even though the effect is similar to our experimental measurements, the general behavior is completely different. Basically, such a model presents a shortcoming at $H_a=H_{C1}$. Indeed, the delta function source of the generalized London equation was replaced by a spatially homogeneous vortex density term, valid only for $H_a \gg H_{C1}$ but failing close to H_{C1}.

In order to account for our not constant modulation period, the abrupt discontinuity at H_{C1} must be replaced by a continuous entrance or exit of vortices, i.e., by a continuous contribution of vortices to the supercurrent for both increasing and decreasing magnetic fields. In this paper, we are going to follow a simpler approach, which however can explain much more easily all our experimental data. We use the Fraunhofer diffraction formula for I_{Cj} [Eq. (1)], replacing the external applied flux with the effective magnetic flux sensed by the junction. It accounts for the influence of the electrode vortices and stray fields of the continuous Meissner currents shielding the flux-free regions.

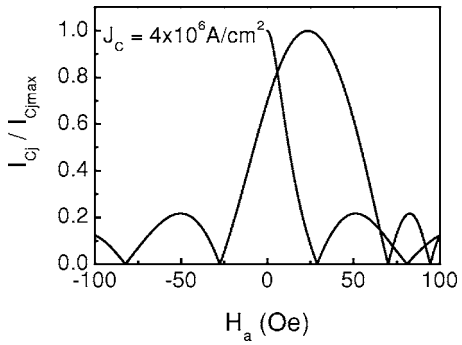

FIG. 8. Calculated $I_{Cj}(H_a)$ dependence for a 700 nm wide GBJ, placed 10 μm away from the electrode (500 μm wide) edge. In the calculations, we have used $J_C=4\times10^6$ A/cm^2 (corresponding to the typical critical current density of our films at $T=77$ K), a thickness $d=120$ nm and $\lambda=270$ nm.

To estimate $H_{\rm eff}$ in our design configuration, we assume that the main contribution to the field at the junction position is given by the large common electrode [Fig. 1(a)]. We then calculate the field profiles inside and outside the electrode and for both increasing and decreasing directions, by using Eqs. (2) and (3) (Fig. 1). Finally, we use the simulated $H_{\rm eff}$ values 10 μm far from the electrode edge (dashed line in Fig. 1), which corresponds to the physical distance between the junction and the electrode in our pattern geometry.

In Fig. 8, we show the calculated $I_{Cj}(H_a)$ behavior for a 700 nm wide junction. In the calculation, we have first increased the magnetic field from 0 Oe to 100 Oe and then decreased H_a from 100 Oe to −100 Oe. The agreement with the experimental curve shown in Fig. 4 is very good, also considering that no fitting parameters have been used. In assigning parameters, we have used experimental values, including a film critical current density $J_C=4\times10^6$ A/cm^2, which is the typical value for our $YBa_2Cu_3O_{7-x}$ films at $T=77$ K, a London penetration depth $\lambda=270$ nm, a film thickness of 120 nm and an electrode width of 500 μm, like in our device geometry.

In Fig. 9, we show the $I_{Cj}(H_a)$ behaviors of a 1 μm wide GBJ, calculated for decreasing H_a, from $H_{max}=5$, 10, 20, 30,

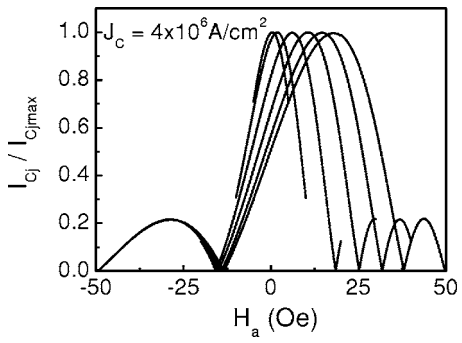

FIG. 9. Calculated $I_{Cj}(H_a)$ dependencies for a 1 μm wide GBJ, placed 10 μm away from the electrode edge. The magnetic field is decreased from $H_{max}=5$, 10, 20, 30, 40, and 50 Oe, respectively, to $-H_{max}$. In the calculations, we have used $J_C=4\times10^6$ A/cm^2 (corresponding to the typical critical current density of our films at $T=77$ K), $\lambda=270$ nm and a thickness $d=120$ nm.

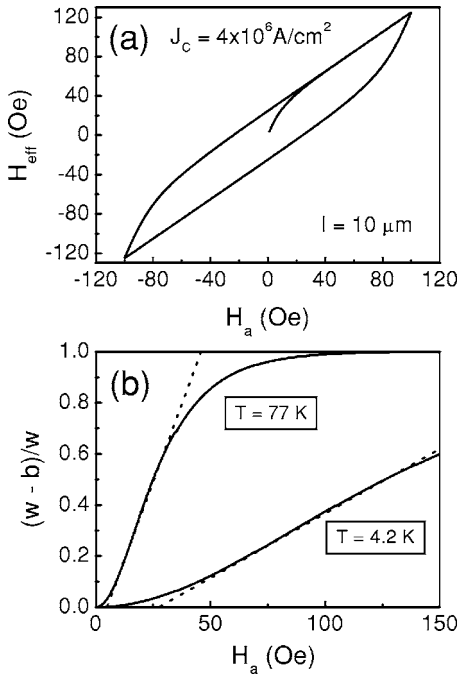

FIG. 10. (a) Hysteretic behavior of the effective magnetic field sensed by the junction as a function of Ha; (b) normalized dependence of the vortex penetration length on the applied magnetic field at $T=77$ K and $T=4.2$ K. Dotted lines are extrapolations through the inflection points to estimate the threshold magnetic field values.

40, and 50 Oe, respectively, to $-H_{\max}$. It is worth noting that the theoretical approach alone,[24] describing the magnetization of a thin strip in perpendicular magnetic fields, is able to account for all the experimental results shown in Fig. 5, with a very good agreement.

In terms of the present model, the nonconstant period and the shifted H_{peak} can be explained as the result of the hysteretic magnetization of the thin film electrodes, as can be seen in Fig. 10(a), where the effective magnetic field, calculated at 10 μm from the electrode edge, is shown for H_a sweeping from 0 to $H_{\max}$, from $H_{\max}$ to $-H_{\max}$ and finally from $-H_{\max}$ to $H_{\max}$. Curves are clearly nonlinear, reproducing the demagnetization effects of the transverse geometry. It is worth noting that the Meissner contribution alone (without vortex entry) would lead to an $I_{Cj}(H_a)$ dependence, characterized by a modulation period ΔH in agreement with the expression $1.84\Phi_0/w^2$, typically used to account for flux focusing effects.[16]

The model is also able to explain the threshold magnetic field values measured at $T=77$ K (of the order of 3 Oe) and at $T=4.2$ K (about 30 Oe). In Fig. 10(b), the normalized penetration length of vortices into the electrode, $(w\text{-}b)/w$ (which affects the effective field sensed by the junction), is reported for $J_C=4\times10^6$ A/cm^2 ($T=77$ K) and $J_C=2\times10^7$ A/cm^2 ($T=4.2$ K). As can be easily seen, at $T=77$ K, vortices enter the thin film for fields much smaller than in the case of $T=4.2$ K. Extrapolating $(w\text{-}b)/w$ by a straight line through the inflection point, we estimate an effective threshold value of about 4 Oe at $T=77$ K and 25 Oe at $T=4.2$ K, in qualitative agreement with our experimental values. It is worth noting that these values, like the H_{peak} shift, only depend on the magnetization of the nearby electrode and are independent of the junction width, in agreement with our experimental measurements.

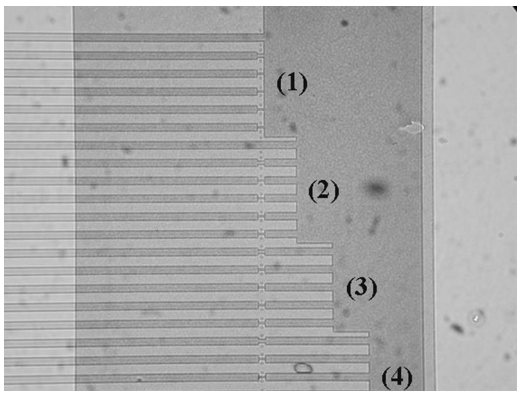

FIG. 11. Optical microscope photograph of the sample used to investigate the influence of electrodes. The junctions are placed at four different distances from the electrodes.

In Ref. 7, sharp discontinuities, whose field position was characterized by a 1/width dependence, also appeared in the $I_{Cj}(H_a)$ curves. The authors interpreted such jumps and the consequent shift in the $I_{Cj}(H_a)$ pattern as being due to the entrance or exit of individual vortices close to the junction, which decreased or increased, respectively, the surface current density at the junction. However, we have never observed these jumps in our samples. The absence of such discontinuities is also consistent with the assumption that our submicron junctions are influenced by a collective effect of several long range interacting Pearl-like fluxons (bundles), trapped inside the electrode, more than the result of the interaction of individual vortices with the junction. It should also be considered that the width of our junctions is comparable with $2\lambda_L$, so vortices tend not to enter within a distance of about 2–3 μm from the junction, which is the typical length of the track narrowed by FIB.

The long range interaction of several vortices with the junction barrier, also accounts for the reproducibility of our $I_{Cj}(H_a)$ dependencies, showing exactly the same behavior after several days. Indeed, even though the position and the interaction of a single vortex can change every time, the influence of a large number of fluxons is statistically averaged, giving a reproducible contribution.

The vortex density coupled to the junction is of course strongly dependent on the electrode geometry. In order to investigate the effects of the geometrical pattern configuration and to confirm our theoretical approach, we have analyzed the $I_{Cj}(H_a)$ curves of several submicron junctions placed at four different distances from the large common electrode (Fig. 11), $l=10$ μm (region 1), 110 μm (region 2), 210 μm (region 3), and 310 μm (region 4). Figure 12 shows the $I_{Cj}(H_a)$ dependencies for two submicron junctions of regions 1 and 4, respectively, at both $T=4.2$ K and $T=77$ K.

The effect of the junction configuration is clearly visible and is summarized in Fig. 13(a), where the hysteresis (H_{peak}), corresponding to junctions from the four different regions are reported as a function of $H_{\max}$ at $T=77$ K.

For a fixed maximum applied magnetic field, the shift of H_{peak} decreases with the distance l of the junction from the

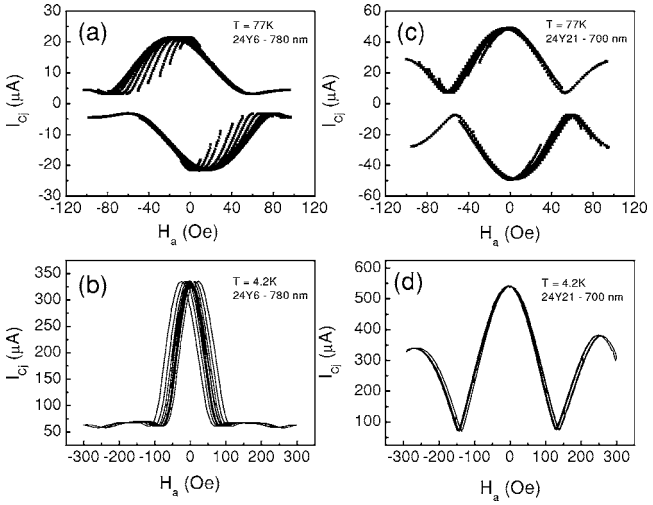

FIG. 12. $I_{Cj}(H_a)$ dependencies of two submicron junctions: (a), (b) from region 1, 10 μm from the electrode; (c), (d) from region 4, 310 μm from the electrode. Curves refer to $T=77$ K (at the top) and $T=4.2$ K (at the bottom).

electrode. Region 1 and 4 are then characterized by the largest and smallest hysteresis, respectively. Indeed, for larger l values, there is a smaller vortex contribution giving more linear $H_{\mathrm{eff}}(H_a)$ dependencies and, as a result, narrower hysteresis in the magnetization curves. This feature is well explained by Eqs. (2) and (3), as shown in Fig. 14(a), where curves corresponding to different distances l have been obtained by cutting the stray field at the proper positions [Fig. 1(b)].

In Fig. 13(b), the central modulation periods measured in GBJs with a nominal 2 μm width are shown as a function of H_{max}, for the first three regions. Curves have been normalized to their values at 80 Oe in order to make them independent of the spread in junction width, caused by photolithographic and etch processes. In absolute values, all the experimental periods are larger than the ones predicted by the Rosenthal formula,[16] as expected considering that the field enhancement at the grain boundary is counterbalanced by the stray field of vortices coupled, in the opposite direction, to the junction. The flux focusing effect is then reduced. A better agreement with the $1.84\Phi_0/w^2$ expression[16] is observed in the case of junctions 10 μm far from the electrode (when the flux focusing is maximum) and only for small maximum applied magnetic fields (when a few vortices penetrates the superconducting electrode).

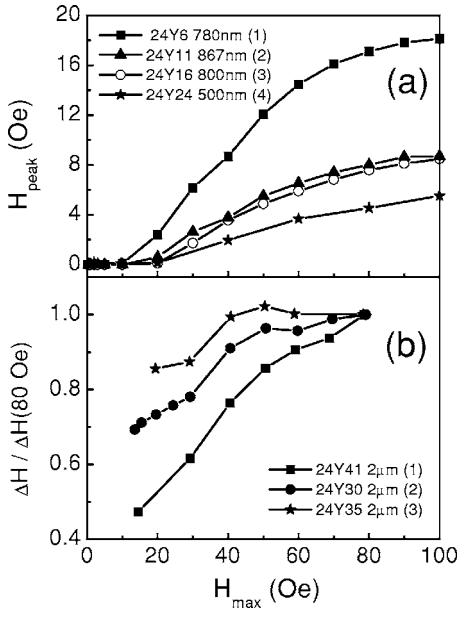

FIG. 13. Dependence of the hysteresis (a) and the central period (b) on the maximum applied magnetic field H_{max}, for several junctions at different distances from the electrodes. Data refer to $T=77$ K.

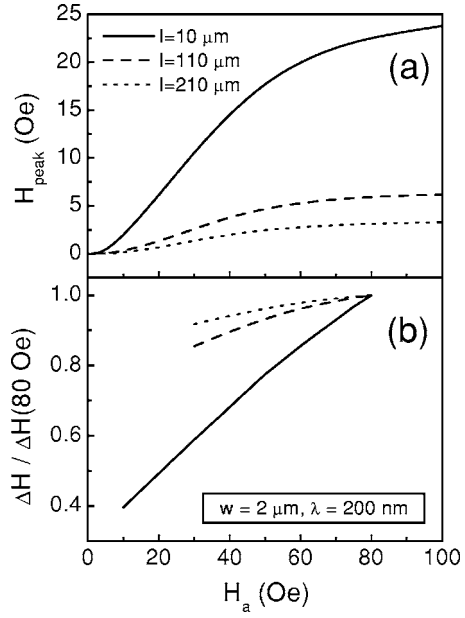

FIG. 14. Theoretical dependence of (a) the hysteresis and (b) the central period on the maximum applied magnetic field H_{max}, for junctions located at different distances from the electrodes $l=10$ μm, 110 μm, and 210 μm. Data refer to $T=77$ K.

In Fig. 14(b), we show the normalized theoretical dependence of the modulation period on H_{max}, for three GBJs, 2 μm wide, placed at distances $l=10$ μm, 110 μm, and 210 μm from the electrode. Theoretically, we expect a smaller modulation period for smaller l, since demagnetization effects (due to the close electrode) increase and, at the same time, there is a larger vortex contribution, which leads to strong nonlinear magnetization curves. It is worth noting that the slope of simulated curves well accounts for our experimental results. Finally we point out that, in contrast to what is reported in the literature,[3] the maximum value of the critical current at H_{peak}, $I_{Cj\mathrm{max}}$, does not show a clear decrease with increasing H_{max}. On the contrary, at $T=4.2$ K, $I_{Cj\mathrm{max}}$ is constant in the whole H_{max} range, from $H_{\mathrm{max}}=0.1$ Oe to $H_{\mathrm{max}}=350$ Oe while at $T=77$ K, $I_{Cj\mathrm{max}}$ is characterized by a plateau up to H_{max} values of the order of 80 Oe with a decrease only for larger fields. In Fig. 15, this behavior is shown for a 780 nm wide GBJ at $T=77$ K. The constant $I_{Cj\mathrm{max}}$ is what is expected since the junction probes an effective field given by three contributions, external field, additional field due to Meissner shielding currents and stray

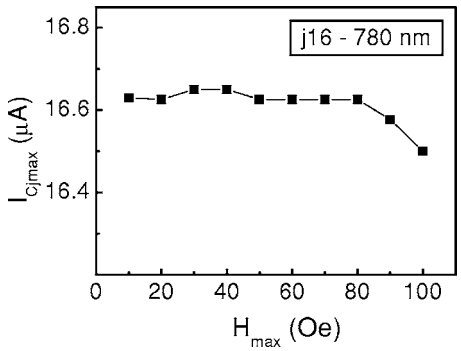

FIG. 15. Dependence of the maximum value of the critical current at H_{peak} as a function of H_{max}. Data refer to a 780 nm wide GBJ at T=77 K.

field of Pearl-like vortices. The decrease of $I_{Cj\max}$ at fields larger than 80 Oe may be related to the presence of vortices in the superconducting banks close to the junctions (at distances of the order of $\lambda_{eff}=2\lambda^2/d$). Their effect is then not only to modify the effective magnetic field sensed by the GBJ but also to depress the superfluid density and the current distribution in the junction barrier.

V. CONCLUSIONS

In conclusion, we have observed a strong influence of electrodes on the magnetic properties of submicron bicrystal grain boundary junctions. The large magnetic fields, of the order of tens of Oersted, required to modulate their critical currents, lead to the trapping, into the film, of a large number of Pearl-like vortices whose dynamics is regulated by the following factors: the Lorentz force with the Meissner screening currents, the repulsive interaction with the other vortices and the attractive interaction, of the Bean-Livingston type, with image vortices. Moreover, above all at low temperatures, there is a strong "plastic interaction"[30] with structural pinning sites, which generates a vortex gradient into the electrodes. The coupling of such long range interacting fluxons with the junction barrier, together with the hysteresis in the electrode magnetization, accounts for the asymmetric and irreversible $I_{Cj}(H_a)$ dependencies observed experimentally. Our analysis not only gets an insight into the physics and dynamics of Abrikosov vortices near a Josephson junction (important for both basic physics and for applications like SQUID magnetometers) but also gives some clue to potential new vortex-based applications like memory cells.

ACKNOWLEDGMENTS

This work has been partially supported by the ESF Network "Pi-shift," by MIUR under the projects 3, cluster "Componentistica Avanzata," and by EPSRC. The authors gratefully acknowledge E. Sarnelli for useful suggestions and C. Salinas for his technical support in our experiments. F.L. thanks E. Mezzetti for fruitful discussions.

[1] A. Barone and G. Paternò, *Physics and Applications of the Josephson Effect* (Wiley, New York, 1982).
[2] M. Daumling, E. Sarnelli, P. Chaudhari, A. Gupta, and J. Lacey, Appl. Phys. Lett. **61**, 1355 (1992).
[3] B. M. Hinaus, R. D. Redwing, and M. S. Rzchowski, Appl. Phys. Lett. **70**, 517 (1997).
[4] J. Z. Sun, W. J. Gallagher, and R. H. Koch, Phys. Rev. B **50**, 13664 (1994).
[5] N. Uchida, K. Enpuku, Y. Matsugaki, S. Tomita, F. Irie, and K. Yoshida, J. Appl. Phys. **54**, 5287 (1983).
[6] R. G. Humphreys and J. A. Edwards, Physica C **210**, 42 (1993).
[7] E. E. Mitchell, C. P. Foley, K. -H. Muller, and K. E. Leslie, Physica C **321**, 219 (1999).
[8] A. I. D'yachenko, Physica C **213**, 167 (1993).
[9] D. J. Van Harlingen, Rev. Mod. Phys. **67**, 515 (1995).
[10] C. C. Tsuei and J. R. Kirtley, Rev. Mod. Phys. **72**, 969 (2000).
[11] H. Hilgenkamp and J. Mannhart, Rev. Mod. Phys. **74**, 485 (2002).
[12] R. Gross, in *Interfaces in High-Tc Superconducting Systems*, edited by S. L. Shinde and D. A. Rudman (Springer-Verlag, New York, 1992), p. 176.
[13] E. Sarnelli and G. Testa, Physica C **371**, 10 (2002).
[14] A. Gurevich and E. A. Pashitskii, Phys. Rev. B **57**, 13878 (1998).
[15] B. H. Moeckly, D. K. Lathrop, and R. A. Buhrman, Phys. Rev. B **47**, 400 (1993).
[16] P. A. Rosenthal, M. R. Beasley, K. Char, M. S. Colclough, and G. Zaharchuk, Appl. Phys. Lett. **59**, 3482 (1991).
[17] G. Testa, A. Monaco, E. Sarnelli, A. D'Agostino, D. -J. Kang, E. J. Tarte, S. H. Mennema, C. Bell, and M. G. Blamire, Supercond. Sci. Technol. **7**, 287 (2004).
[18] G. Testa, A. Monaco, E. Esposito, E. Sarnelli, D. -J. Kang, S. H. Mennema, E. J. Tarte, and M. G. Blamire, Appl. Phys. Lett. **85**, 1202 (2004).
[19] G. Testa, E. Sarnelli, A. Monaco, E. Esposito, M. Ejrnaes, D. -J. Kang, S. H. Mennema, E. J. Tarte, and M. G. Blamire, Phys. Rev. B **71**, 134520 (2005).
[20] E. Ilichev, M. Grajcar, R. Hlubina, R. P. J. IJsselsteijn, H. E. Hoenig, H. -G. Meyer, A. Golubov, M. H. S. Amin, A. M. Zagoskin, A. N. Omelyanchouk, and M. Y. Kupriyanov, Phys. Rev. Lett. **86**, 5369 (2001).
[21] C. P. Bean and J. D. Livingston, Phys. Rev. Lett. **12**, 14 (1964).
[22] C. P. Bean, Rev. Mod. Phys. **36**, 31 (1964).
[23] E. H. Brandt, Phys. Rev. B **54**, 4246 (1996).
[24] E. H. Brandt and M. Indenbom, Phys. Rev. B **48**, 12893 (1993).
[25] F. Laviano, D. Botta, A. Chiodoni, R. Gerbaldo, G. Ghigo, L. Gozzelino, and E. Mezzetti, Phys. Rev. B **68**, 014507 (2003).
[26] E. H. Brandt, Phys. Rev. B **46**, 8628 (1992).
[27] J. Pearl, Appl. Phys. Lett. **5**, 65 (1964).
[28] G. Carneiro and E. H. Brandt, Phys. Rev. B **61**, 6370 (2000).
[29] K. -H. Muller, E. E. Mitchell, J. Herrmann, D. B. Lowe, C. Andrikidis, A. J. Thorley, C. Foley, and N. Savvides, Physica C **366**, 245 (2002).
[30] G. Blatter, M. V. Feigel'man, V. G. Geshkenbein, A. I. Larkin, and V. M. Vinokur, Rev. Mod. Phys. **66**, 1125 (1994).